Journal of Computational Acoustics

SPECTRAL FINITE ELEMENTS FOR COMPUTATIONAL AEROACOUSTICS USING ACOUSTIC PERTURBATION EQUATIONS

ANDREAS HÜPPE
MANFRED KALTENBACHER
Chair of Applied Mechatronics,
Alps Adriatic University,
Klagenfurt, Austria
andreas.hueppe@aau.at
http://am.aau.at

Received (Day Month Year)
Revised (Day Month Year)

The paper in hand addresses the application of the spectral finite element (FE) method to problems in the field of computational aeroacustics (CAA). We apply a mixed finite element approximation to the acoustic perturbation equations, in which the flow induced sound is modeled by assesing the imapct of a mean flow field on the acoustic wave propagation. We show the properties of the approximation by numerical benchmarks and an application to the CAA problem of sound generated by an airfoil.

Keywords: Finite Elements; Aeroacoustics; Perturbation Equations.

1. Introduction

Many numerical methods have been proposed in the field of computational aeroacoustics (CAA) most of which rely on a hybrid approach in which the sound radiation is calculated based on sources obtained from a preceding flow field computation. Integral methods like Ffwocs Williams-Hawkings or the Kirchhoff method have been proposed which are specially well suited for free field radiation problems due to their low computational complexity. Among the volume discretization methods, the finite element (FE) method is one of the most general and established numerical schemes. The numerical simulation of flow induced sound using the wave equation in combination with Lighthill's acoustic analogy[1] is well established and widely used in many different scenarios[2,3,4,5]. For acoustic propagation in the presence of a (non-uniform) mean flow or compressible, non-isentropic media, formulations based on the linearized Euler equations and perturbed acoustic equations can be utilized. These equations are mostly solved by using numerical schemes like finite differences (FD) or discontinuous Galerkin (DG) methods [6,7,8]. Within the paper in hand we focus on a spectral finite element solution of the acoustic perturbation equations (APE) given in [5]. As the standard finite element method does not yield stable solutions we use a mixed variational formulation as introduced in [9] for linear acoustics which we extend to numerically solve for

APE.

The rest of the paper is structured as follows. In section two we discuss the governing equations as well as the corresponding aeracoustic source terms. Next we derive the variational formulation for APE and investigate its properties in terms of accuracy and stability in section four. Afterwards we present a modified formulation which yields a better stability and finally demonstrate in section six the applicability of the scheme to aeroacoustic problems.

2. Aeroacoustic formulations

The derivation of the acoustic perturbation equations is based on the linearized Euler equations in which the unknown quantities are split into their mean and fluctuating parts

$$f(\mathbf{x},t) = \overline{f}(\mathbf{x}) + f'(\mathbf{x},t) \;\; ; \;\; \overline{f}(\mathbf{x}) = \lim_{T\to\infty} \frac{1}{T} \int_{t_0}^{t_0+T} f(\mathbf{x},t)\, \mathrm{d}t \; .$$

For the density ρ, the pressure p and the velocity $\mathbf{u}$ we thereby obtain

$$\rho = \overline{\rho} + \rho' \;\; ; \;\; \mathbf{u} = \overline{\mathbf{u}} + \mathbf{u}' \;\; ; \;\; p = \overline{p} + p' \; .$$

By using a source term filtering technique to ensure that only acoustic eigenmodes of the system are excited [5] it is possible to derive the perturbation equations which include convective effects of a present mean flow

$$\frac{\partial p'}{\partial t} + \overline{c}^2 \nabla \cdot (\overline{\rho}\, \mathbf{u}') + \overline{c}^2 \nabla \cdot (\mathbf{u}' \frac{p'}{\overline{c}^2}) = \overline{c}^2 q_\mathrm{c} \; , \tag{1}$$

$$\frac{\partial \mathbf{u}'}{\partial t} + \nabla(\overline{\mathbf{u}} \cdot \mathbf{u}') + \nabla \left(\frac{p'}{\overline{\rho}} \right) = \mathbf{q}_\mathrm{m} \; . \tag{2}$$

In the following we refer to p' as the acoustic pressure and to $\mathbf{u}'$ as the acoustic particle velocity.

In the special case of a vanishing mean flow,$\overline{\mathbf{u}} = \mathbf{0}$, and spatially constant speed of sound $\overline{c} = c_0$ and density $\overline{\rho} = \rho_0$, we directly obtain the conservation equations of linear acoustics which can be transformed to get to the acoustic wave equation in its pressure formulation

$$\frac{1}{c_0^2} \frac{\partial^2 p'}{\partial t^2} + \Delta p' = q_\mathrm{w} \; . \tag{3}$$

To compute the aeroacoustic source terms in above equtions one has to rely on an acoustic analogy which uses flow quantities to formulate acoustially relevant source terms.

One of the most general and established analogies is given by Lighthill for the acoustic wave equation [1]. The right hand side of (3) then reads as

$$q_\mathrm{w} = \frac{\partial^2 T_{ij}}{\partial x_i \partial x_j} \;\; ; \;\; i,j \in [1,2,3] \; , \tag{4}$$

in which T_{ij} denote the components of the Lighthill tensor $[T]$ which can be approximated as $T_{ij} \approx \rho u_i^{\mathrm{f}} u_j^{\mathrm{f}}$ were $\mathbf{u}^{\mathrm{f}}$ denotes the flow velocity obtained e.g. by a numerical solution of the flow field.

The source term for APE is based on the Lamb vector[10] given by $\mathbf{L} = \boldsymbol{\omega}^f \times \mathbf{u}^f$. Here, $\boldsymbol{\omega}^f$ denotes the vorticity of the fluid and is defined as $\boldsymbol{\omega}^f = \nabla \times \mathbf{u}^f$. For problems in which most of the sound is generated by vortices in the flow field, the sources of the system (1) and (2) can be given as

$$\begin{aligned} q_{\mathrm{c}} &= 0 \\ q_{\mathrm{m}} &= -\left(\boldsymbol{\omega}^f \times \mathbf{u}^f\right)' = -\mathbf{L}' \ . \end{aligned} \tag{5}$$

The vector $\mathbf{L}'$ is referred to as the perturbed Lamb vector and is computed as $\mathbf{L}' = \left(\boldsymbol{\omega}^f \times \mathbf{u}^f\right) - \left(\overline{\boldsymbol{\omega}^f \times \mathbf{u}^f}\right)$.

3. Weak formulation and FE discretization

For a finite element method it is essential to find a variational formulation for the given partial differenctial equation (PDE). Therewith, the wave equation according to (3) results in [11]

$$\frac{1}{c_0^2}\int_\Omega \varphi \frac{\partial^2 p'}{\partial t^2}\,\mathrm{d}\Omega + \int_\Omega \nabla\varphi\cdot\nabla p'\,\mathrm{d}\Omega = -\int_\Omega \nabla\varphi\cdot(\nabla\cdot[T])\,\mathrm{d}\Omega + \int_\Gamma \varphi\frac{\partial p'}{\partial \vec{n}}\,\mathrm{d}\Gamma\ , \tag{6}$$

with $\nabla\cdot[T]$ the divergence of the Lighthill tensor. Furthermore we assume that the velocity field vanishes at the domain boundary i.e. $\frac{\partial T_{ij}}{\partial x_j} n_i = 0$. Now it is possible to apply the finite element (FE) method to (6) in which the unknown quantity as well as the test function φ are thought to be within the Sobolev space H^1.[a]

For the derivation of the variational formulation of APE we restrict ourself to the case of a spatially constant mean flow $\overline{\mathbf{u}} = \mathbf{u}_0$. Initially we multiply (1) with a test function φ and (2) with a vectorial function $\boldsymbol{\psi}$. An integration over the computational domain leads to

$$\frac{1}{\rho_0 c_0^2}\frac{\partial}{\partial t}\int_\Omega p'\ \varphi\ \mathbf{d}\Omega + \int_\Omega \nabla\cdot\mathbf{u}'\varphi\ \mathbf{d}\Omega + \frac{1}{\rho_0 c_0^2}\int_\Omega \mathbf{u}_0\cdot\nabla p'\ \varphi\ \mathbf{d}\Omega = \frac{1}{\rho_0}\int_\Omega q_{\mathrm{c}}\ \varphi\ \mathbf{d}\Omega\ , \tag{7}$$

$$\rho_0\frac{\partial}{\partial t}\int_\Omega \mathbf{u}'\cdot\boldsymbol{\psi}\ \mathbf{d}\Omega + \rho_0\int_\Omega (\mathbf{u}_0\cdot\nabla)\,\mathbf{u}'\cdot\boldsymbol{\psi}\ \mathbf{d}\Omega + \int_\Omega \nabla p'\cdot\boldsymbol{\psi}\ \mathbf{d}\Omega = \rho_0\int_\Omega \mathbf{q}_{\mathrm{m}}\cdot\boldsymbol{\psi}\ \mathbf{d}\Omega\ . \tag{8}$$

Furthermore we perform an integration by parts on the second term in (7) which reads as

$$\int_\Omega \nabla\cdot\mathbf{u}'\varphi\ \mathbf{d}\Omega = -\int_\Omega \mathbf{u}'\cdot\nabla\varphi\ \mathbf{d}\Omega + \int_\Gamma \mathbf{u}'\cdot\mathbf{n}\ \varphi\ \mathbf{d}\Gamma\ . \tag{9}$$

[a] H^1 is the Sobolev space,i.e. the space of square integrable functions whose first derivatives in a weak sense are also square integrable[12]

Unless explicitly noted, the boundary integral is assumed to be zero which corresponds to a sound hard wall [13].

Even for the case of vanishing mean flow it is not trivial to obtain a stable finite element method due to the violation of the *Ladyzhenskaya-Babuška-Brezzi* (or inf-sup) condition [14]. One has to use either a discontinuous Galerkin (DG) scheme or a mixed formulation in which the unknowns are defined in different Sobolev spaces.

To define the functional spaces we follow [9] and assume a domain, discretized by N quadrilateral or hexahedral finite elements K, $\Omega = \cup_{j=1}^{N} K_j$. Furthermore, there is a bijective mapping $\mathbf{F_j}$ to transform the grid element K_j to the reference element $\hat{K}_j$. Then the discrete spaces of approximation are defined as

$$p'_h, \varphi_h \in U_h^k = \left\{ q \in H_0^1 \;\middle|\; q|_{K_j} \circ F_j \in Q^k(\hat{K}_j) \text{ and } q = 0 \text{ on } \Gamma \right\} \tag{10}$$

$$\mathbf{u}'_h, \boldsymbol{\psi}_h \in V_h^k = \left\{ \mathbf{w} \in [L_2]^d \;\middle|\; \frac{1}{|\mathcal{J}_j|} \mathcal{J}_j \; \mathbf{w}|_{K_j} \circ F_j \in \left[Q^k(\hat{K}_j) \right]^d \right\} \quad . \tag{11}$$

In (10) and (11), $\mathcal{J}_j$ denotes the Jacobian of element K_j and $Q^k(\hat{K}_j)$ the set of Lagrange polynomials of degree k and dimension d on $\hat{K}_j$. Furthermore, L_2 is the space of Lebesque square integrable functions [12]. Thereby the acoustic particle velocity $\mathbf{u'}$ is approximated discontinuously from element to element which is similar to a DG formulation.

It is important to notice, that the space V_h^k is defined with the $H(\mathbf{div})$-conforming Piola transform [15]. Therefore, the mapping of the grid element to the reference element is defined by $\mathbf{u}_h = 1/|\mathcal{J}_j| \; \mathcal{J}_j \hat{\mathbf{u}}_h$. The usage of this mapping in combination with a spectral element approximation[16,9] enables a very efficient implementation of the resulting scheme [17].

In the initial approach we applied the above choice of functional spaces directly to the variational formulation of APE and investigate its accuracy and stability by the means of the following numerical examples.

4. Verification and stability test

As a verification example we choose a setup introduced in [18] as depicted in Fig. 1a. At $t = 0$ we prescribe an acoustic pressure field given by

$$p'(t=0) = \exp\left(\ln(2) \frac{x^2 + (y+75)^2}{25} \right) \; ,$$

while setting $\mathbf{u'}(t = 0)$ to be zero. During the pulse propagation, we record the acoustic pressure for different times along the monitoring line plotted in Fig. 1a. For the computation we choose a uniform flow velocity of $\mathbf{u}_0 = (0.5\overline{c}, 0)^T$ resulting in a Mach number $M_x = 0.5$. The domain is discretized by second order spectral elements with an edge length of $h = 1$m and a fourth order Runge-Kutta time stepping scheme is used. The pressure distribution along the monitoring line is given in Fig. 1b for $t = 60$s. Analytical and the numerical solutions match well, which validates our approach.

To investigate the stability the setup is changed such that the domain is assumed to be bounded by sound-hard walls. The solution becomes instable after the wave impinges on the

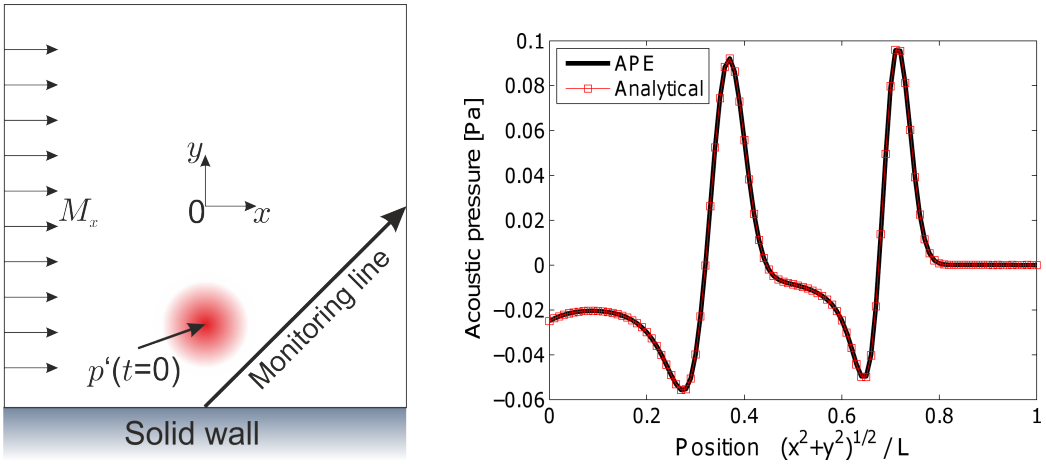

(a) Sketch of computational setup

(b) Computed acoustic pressure and analytical solution along the monitoring line with length L for $t = 60$s

Fig. 1: Sketch of setup used for verification of the scheme and comparison of computational results to analytical solution.

domains boundary (Fig. 2 (*left*)). Similar instabilities have been observed for other setups especially in case of higher Mach numbers and distorted meshes. Therefore, the following attempts were made to stabilize the solution.

5. A modified formulation

The convective term in (8), i.e. the second integral, requires the computation of the derivative of the aocustic particle velocity. This operation is problematic because the functional space of the particle velocity is the discontinuous space L^2. Therefore we utilize the idea of the discontinuous Galerkin method and add a numerical flux term to (8).

Assume two adjacent elements K_1 and K_2 with a common boundary Γ_{12} then a central flux could be formulated as [6]

$$\begin{aligned}\int_{K_1} (\mathbf{u}_0 \cdot \nabla)\, \mathbf{u}'_{K_1} \cdot \boldsymbol{\psi}_{K_1}\, \mathbf{d}K \approx & -\int_{K_1} \mathbf{u}'_{K_1}\, (\mathbf{u}_0 \cdot \nabla) \cdot \boldsymbol{\psi}_{K_1}\, \mathbf{d}K \\ & + \frac{1}{2}\int_{\Gamma_{12}} ((\mathbf{u}_0 \cdot \mathbf{n}_{K_1})\ \mathbf{u}_{K_1} - (\mathbf{u}_0 \cdot \mathbf{n}_{K_2})\, \mathbf{u}_{K_2}) \cdot \boldsymbol{\psi}_{K_1}\, \mathbf{d}\Gamma \\ & = a(\mathbf{u}', \boldsymbol{\psi})\end{aligned} \tag{12}$$

On the obtained bilinear form $a(\mathbf{u}', \boldsymbol{\psi})$ we performing a reverse integration by parts which

leads to

$$a(\mathbf{u}', \boldsymbol{\psi}) = \int_{K_1} (\mathbf{u}_0 \cdot \nabla)\, \mathbf{u}'_{K_1} \cdot \boldsymbol{\psi}_{K_1}\, \mathbf{d}K \\ -\frac{1}{2} \int_{\Gamma_{12}} ((\mathbf{u}_0 \cdot \mathbf{n}_{K_1})\, \mathbf{u}_{K_1} + (\mathbf{u}_0 \cdot \mathbf{n}_{K_2})\, \mathbf{u}_{K_2}) \cdot \boldsymbol{\psi}_{K_1}\, \mathbf{d}\Gamma \tag{13}$$

Therefore by averaging the two expressions (12) and (13) we obtain

$$\int_{K_1} (\mathbf{u}_0 \cdot \nabla)\, \mathbf{u}'_{K_1} \cdot \boldsymbol{\psi}_{K_1}\, \mathbf{d}K \approx \frac{1}{2} \left(\int_{K_1} (\mathbf{u}_0 \cdot \nabla)\, \mathbf{u}'_{K_1}\, \boldsymbol{\psi}_{K_1}\, \mathbf{d}K \right. \\ \left. - \int_{K_1} \mathbf{u}'_{K_1} \cdot (\mathbf{u}_0 \cdot \nabla)\, \boldsymbol{\psi}_{K_1}\, \mathbf{d}K \right) \\ -\frac{1}{2} \int_{\Gamma_{12}} (\mathbf{u}_0 \cdot \mathbf{n}_{K_2})\, \mathbf{u}_{K_2}\, \boldsymbol{\psi}_{K_1} \mathbf{d}\Gamma\ . \tag{14}$$

In addition one can add an explicit penalization term as used in [6] for the DG formulation.

The effect of these changes in the formulation is demonstrated in Fig. 2. On the left side we see the acoustic pressure field at $T = 150$ s calculated by the original formulation and on the right we see the results of our modifield formulation. Obviously the stability of the scheme was improved dramatically. This result also holds for long time simulations and higher, subsonic Mach numbers. It has to be mentioned that the scheme still shows

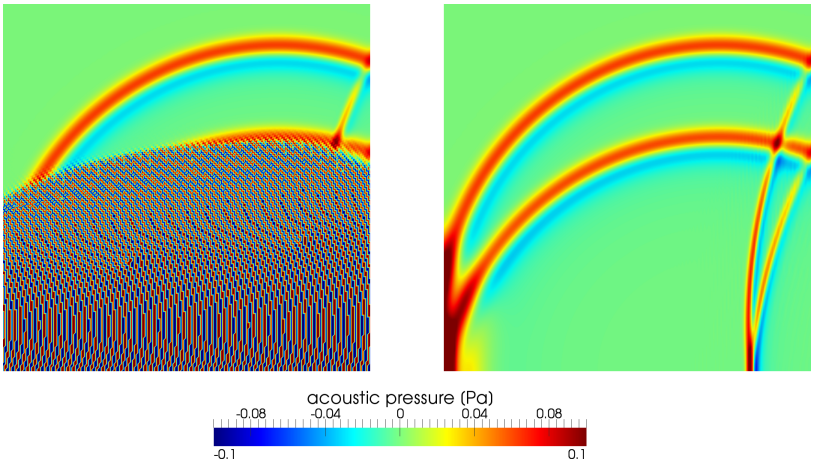

Fig. 2: Stabilizing effect of the modified formulation. Contour plot of the acoustic pressure at $T = 150$ s for the initial formulation (*left*) showing unstable results and the stable results obtained by the proposed ansatz displayed on the right.

instabilities for distorted meshes. We are currently working on further stabilizations and a detailed mathematical analysis.

6. Aeroacoustic computations

The work flow of our approach towards CAA is depicted in Fig. 3. From the results of a flow computation we can calculate the appropriate source terms as given in (4) and (5). Additionally, we can perform the computation required to obtain the right hand side of each formulation. The results are the time dependent aeroacoustic sources on the fluid grid.

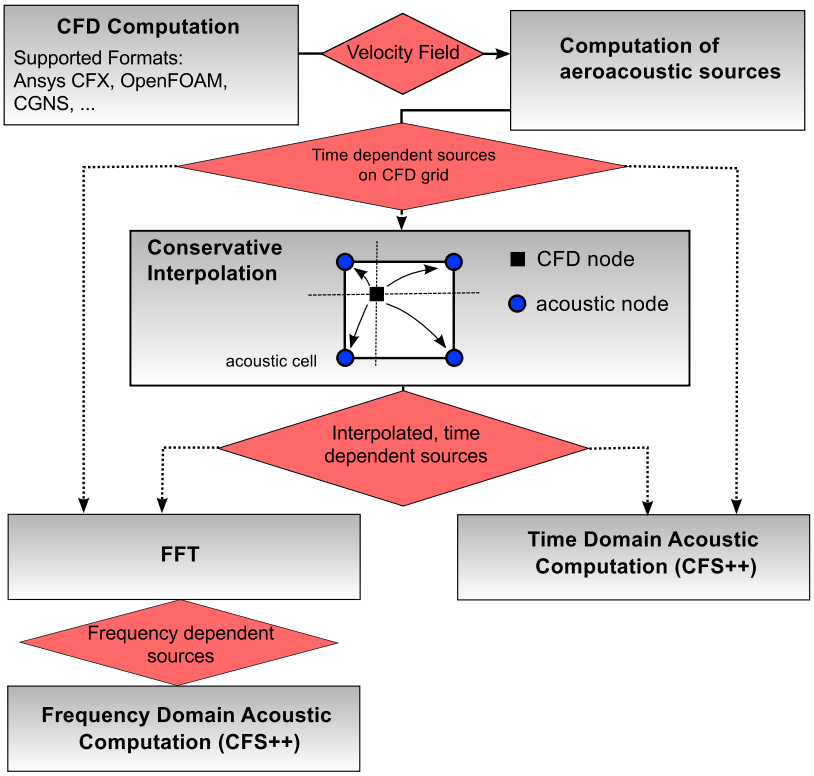

Fig. 3: Toolchain of hybrid aeroacoustic computations

6.1. *Interpolation of source serms*

As the requirements on the computational grid differ significantly for fluid and acoustic computations, it is almost always necessary to transfer the aeroacoustic sources from the fluid grid to a coarser acoustic grid. It is crucial that no energy is lost during this step in order to obtain valid results[11].

The interpolation procedure used here can be split in the following two steps:

(1) For each node in the fluid grid find the element in the acoustic grid in which the node is located

(2) Determine the local coordinates (ξ_k, η_k) of the fluid node with respect to the corresonding reference element and use the elements shape functions N_i to compute the contribution of the fluid nodes value $\mathbf{f}_k^f$ to the degree of freedom $\mathbf{f}_i^a$ of the element taking into account the Piola transform.

6.2. *Co-rotating vortex pair*

To validate our formulation we utilize the co-rotating vortex pair benchmark [11,5] as displayed in Fig. 4a. The two point like vortices are separated by a fixed distance $2r_0$ and have a circulation intensity Γ. The vortices rotate around each other with freqeuncy $\omega = \Gamma/(4\pi r_0^2)$. For this example it is possible to give an analytical expression for the flow field as well as

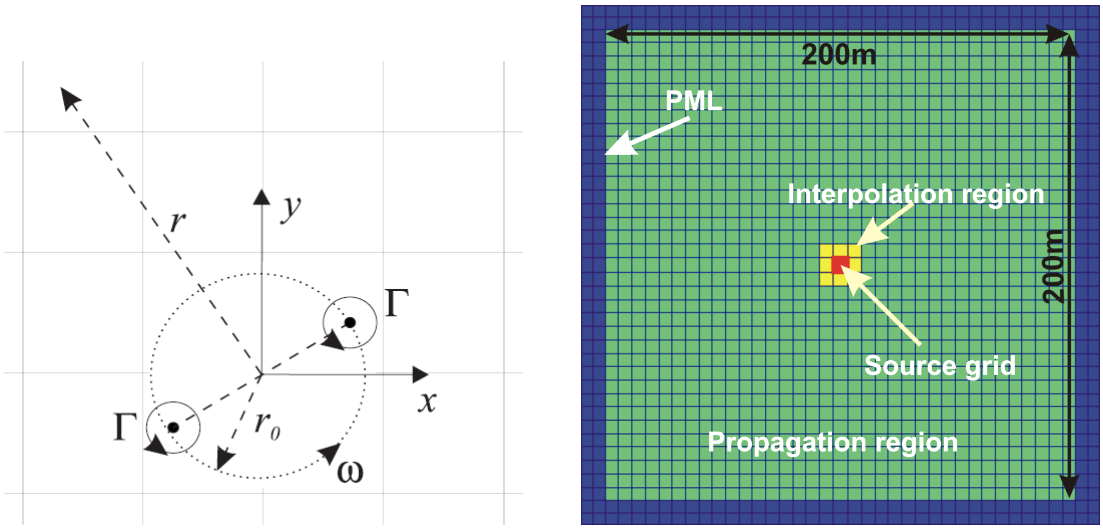

(a) Schematic diagram of co-rotating vortices

(b) Sketch of acoustic domains Ω_a and the source grid Ω_f in the center

Fig. 4: Co-rotating vortices example

for the induced acoustic pressure by using the method of matched asymptotic expansion (MAE) [19].

As the vortices are confined to delta functions, we follow [5] and evaluate a vortex core model based on an Gaussian vorticity distribution with standard deviation $\sigma \approx r_0$. The vortex source term for the APE can be given as

$$\mathbf{q}_\mathrm{m}(\mathbf{r}, t) = -\frac{\Gamma\, \mathbf{e}_r(t)}{8\pi^2\sigma^2 r_0} \sum_{i=1}^{2} (-1)^i \exp\left(-\frac{|\mathbf{r} + (-1)^i\, \mathbf{r}_0(t)|^2}{2\sigma^2}\right) . \tag{15}$$

In (15) we define $\mathbf{r} = (x, y)^T$, $\mathbf{r}_0 = r_0 \mathbf{e}_r$ and $\mathbf{e}_r = (\cos(\omega t), \sin(\omega t))^T$. The resulting source term is computed on a fine computational grid Ω_f with dimensions 8mx8m and an element size $h^f = 0.01$m.

The domain Ω_a of dimenstion 200mx200m for the acoustic field computation with a mesh size h^a of 6m is displayed in Fig. 4b. Additionaly, the source gird Ω_f is displayed in the center of the acoustic domain. It can be seen that almost the complete source grid is included in just one finite element of the acoustic grid. Around the propagation region we define a perfectly matched layer (PML) to avoid reflections at the domain boundary [13].

As a first step we compute the acoustic pressure on a fine grid with element size $h^a = 0.4$m and second order spectral elements. A comparison between analytical pressure field and computed pressure field is shown in Fig. 5. One can see only minor deviations in the two fields. In Fig. 6 the acoustic pressure along a line is plotted for the finer ($h^a = 0.4$ m)

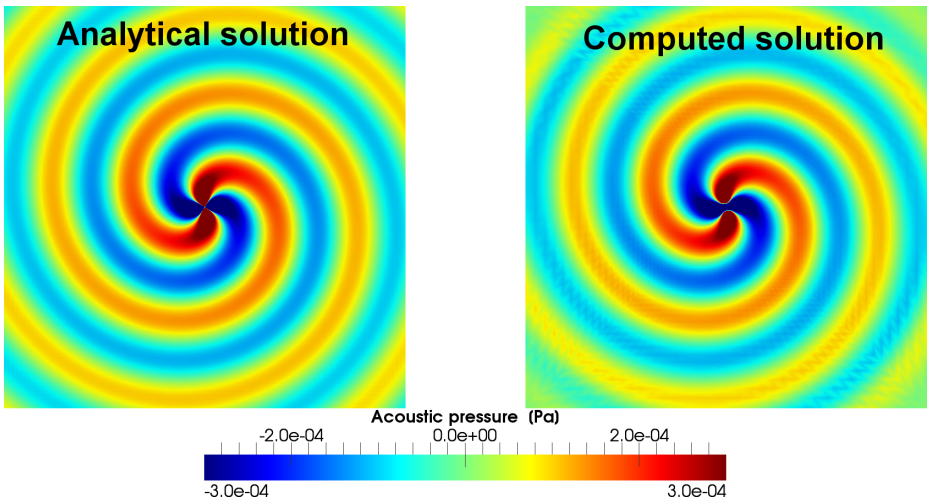

Fig. 5: Sound field generated by a corotating vortex pair. Contour plot of acoustic pressure for analytical solution $h = 0.1$m and computed solution $h^a = 0.4$m

and the coarser grid ($h^a = 6$ m). One can see, that the computed values are in very good agreement to the analytical solution even for the coarse gird.

6.3. *Trailing edge noise*

As a final, practical example we apply the numerical scheme to the setup depicted in Fig. 7. The CFD computation has been carried out at a Mach number of 0.3 and is motivated by the NACA 0012 airfoil test-case[20]. The fluid computation along with aeroacoustic results using Lighthills analogy have been presented in [21]. The aim of the current investigation is to show some of the properties of two aeroacoustic schemes using the wave equation on the one hand and the APE on the other.

Following the work flow, we initially compute the aeroacoustic sources on the CFD grid which leads to right hand sides plotted in Fig. 8. It is obvious that the Lighthill sources show spourious sources which are confined to lines in the fluid grid. This is most likely caused by the combination of two issues. First, to compute the CFD solution a finite

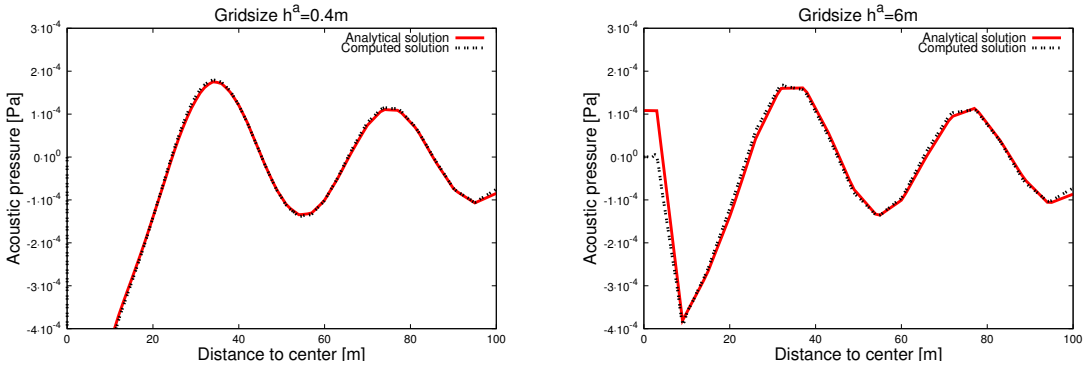

(a) Fine grid (b) Coarse grid

Fig. 6: Comparison of numerical and analytical solution for the corotating vortex pair. Plot along the line from domain center at $(0,0)^T$ to right boundary at $(100,0)^T$

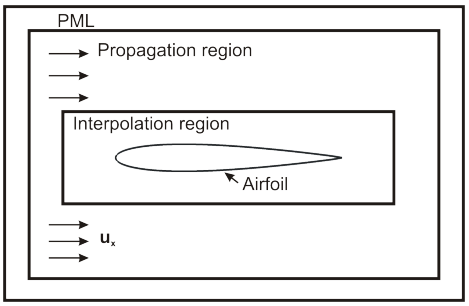

Fig. 7: Schematic diagram of airfoil at Mach 0.3

volume (FV) scheme has been utilized in which the solution may have minor jumps from one element to the other. Secondly the computation of the right hand side integral involves the multiplication of the divergence of the Lighthill tensor by the derivative of the test function which makes the result very sensitive against small deviations in the flow field. Thereby the afore mentioned minor jumps can cause distortions in the field as pictured in Fig. 8a. Still it has to be noted that these spurious sources have a much lower amplitude (factor $1 \cdot 10^2$) then the major source terms. The right hand side field based on the Lamb vector does not show these oscillations and the sound generating vortices can be seen nicely (see Fig. 8b). To investigate if this difference in the sources has an impact on the numerical results, we compare the sound pressure level of the two computations at a monitoring point 0.4cm above the airfoil (see Fig. 10 for the position of the monitoring point). To obtain the results we compute a total time of $T = 0.1$ s with the time step size of the limiting *Courant-Friedrichs-Lewy* (CFL) condition for the fourth order Runge-Kutta scheme used for the APE. The speed of sound is $c_0 = 343$m/s and the acoustic grid is computed to have at least 5 second order elements per wavelength for a frequency of 5kHz which correspond

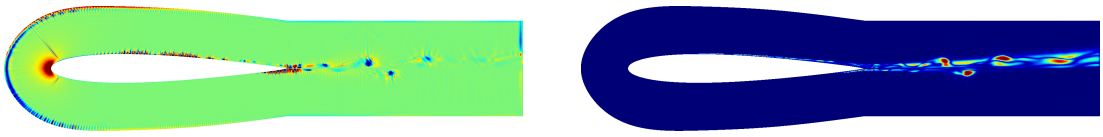

(a) Based on Lighthill tensor
(scaled by a factor of $1 \cdot 10^2$)

(b) Based on Lamb vector
(magnitude scaled by a factor of 10)

Fig. 8: Contour plots of right hand side terms

to $h^a \approx 0.06$m. Depicted in Fig. 9 are the frequency transformed sound pressure levels

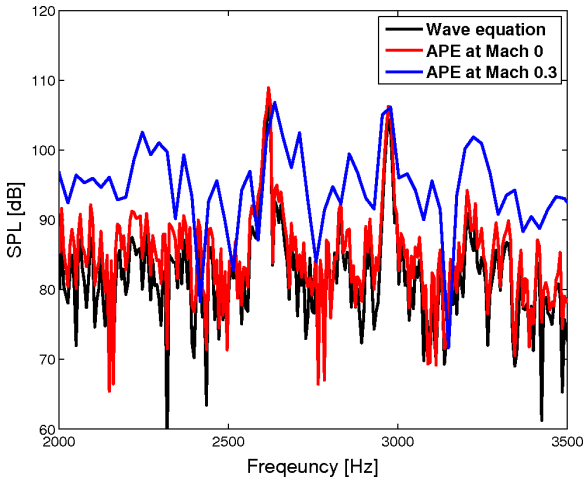

Fig. 9: Sound pressure level 40cm above the airfoil

at the monitoring point above the airfoil for different simulation runs. In the displayed frequency range we notice two significant peaks at 2.6kHz and 3kHz which can be observed in all simulations. One can see, that the results for the wave equation and the APE at zero mean flow are very similar except that the solution of the wave equation is about 3dB lower than the solution with the APE. Possible reasons for this can be related to the implicit time stepping scheme used for the wave equation and/or the spurious source terms mentioned before. In a last simulation run we apply a mean flow of Mach 0.3 to the region of propagation and notice that the calculated SPL is increased over the complete frequency range. Figure 10 shows the acoustic pressure field obtained by APE computations with and without a mean flow velocity. One can see that the acoustic waves are amplified in upstream direction and damped in downstream direction. Right above the airfoil, the two fields are very similar which explains the small differences in the SPLs at the monitoring point.

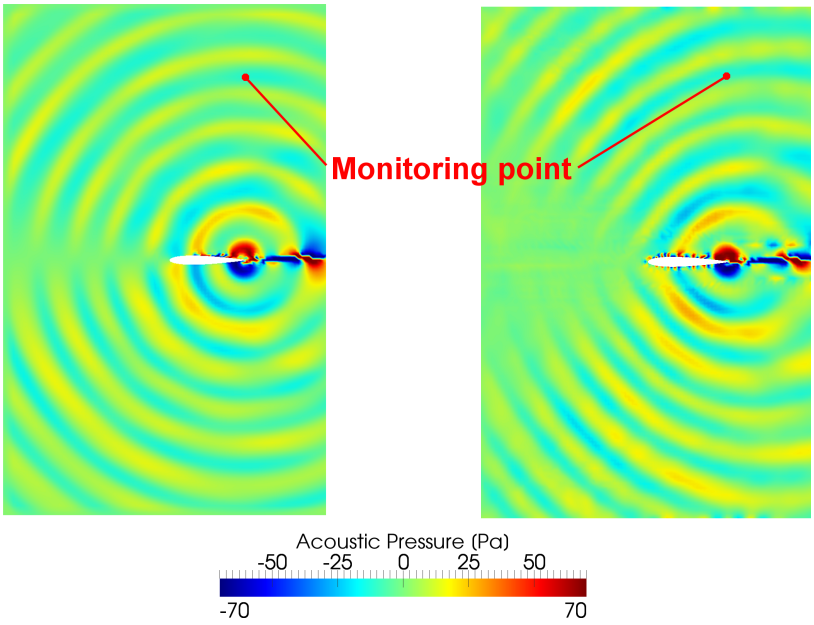

Fig. 10: Contour plot of the acoustic pressure field obtained for the trailing edge noise problem. Comparison of results obtained at Mach 0 (*left*) and for a uniform flow with Mach 0.3 (*right*).

7. Conclusion and outlook

We have presented a spectral finite element approximation to the acoustic perturbation equations based on an mixed variational formulation implemented within the FE framework CFS++[22]. Instabilities which occurred in the initial formulation could be reduced significantly by introducing a numerical flux term as known from DG methods. Furthermore we were able to verify our approach towards computational aeroacoustics including calculation of source terms, interpolation to a coarser acoustic grid of arbitrary element order and finally the acoustic computation. Due to the usage of explicit time stepping schemes the scheme performs very well and the most time consuming part at the moment is the interpolation of source terms in each time step which leaves much room for optimization. One last important issue was noticed during the computations of the airfoil. Even though the elements inside the computational mesh show only minor distortions the setup was very sensitive with respect to stability. This effect shows that the modifications performed so far were not sufficient to obtain a general stable scheme. Addressing this issue will be the main topic in our ongoing research.

Acknowledgment

We would like to thank the Austrian Science Foundation (FWF) for their support by grant I 533-N20 and the Austrian Agency for International Cooperation in Education and Research.

References

1. M. J. Lighthill. On sound generated aerodynamically I. General theory. *Proceedings of the Royal Society of London*, 211:564–587, 1951.
2. G. Link, M. Kaltenbacher, M. Breuer, and M Döllinger. A 2d finite-element scheme for fluid-solid-acoustic interactions and its application to human phonation. *Computer Methods in Applied Mechanics and Engineering*, 198:3321–3334, 2009.
3. Assad A. Oberai, Farzam Roknaldin, and Thomas J.R. Hughes. Computational procedures for determining structural-acoustic response due to hydrodynamic sources. *Computer Methods in Applied Mechanics and Engineering*, 190:345–361, 2000.
4. W. Zhao, S.H. Frankel, and L. Mongeau. Numerical simulation of sound from confined pulsating axisymmetric jets. *American Institute of Aeronautics and Astronautics*, 39:1869–1874, 2001.
5. R. Ewert and W. Schröder. Acoustic perturbation equations based on flow decomposition via source filtering. *Journal of Computational Physics*, 188:365–398, 2003.
6. N. Castel, G. Cohen, and M. Duruflé. Application of discontinuous galerkin spectral method on hexahedral elements for aeroacoustic. *Journal of Computational Acoustics*, 17,2:175–196, 2009.
7. Christophe Bogey, Christophe Bailly, and Daniel Ju. Computation of flow noise using source terms in linearized euler's equations. *AIAA JOURNAL*, 40:235–243, 2002.
8. Jung H. Seo and Young J. Moon. Linearized perturbed compressible equations for low mach number aeroacoustics. *Journal of Computational Physics*, 218:702–719, 2006.
9. G. Cohen and S. Fauqueux. Mixed finite elements with mass-lumping for the transient wave equation. *Journal of Computational Acoustics*, 8:171–188, 2000.
10. Alan Powell. Theory of vortex sound. *The Journal of the Acoustical Society of America*, 36:177 – 196, 1964.
11. M. Kaltenbacher, M. Escobar, I. Ali, and S. Becker. Numerical Simulation of Flow-Induced Noise Using LES/SAS and Lighthill's Acoustics Analogy. *International Journal for Numerical Methods in Fluids*, 63(9):11031122, 2010.
12. Haim Brezis. *Functional Analysis, Sobolev Spaces and Partial Differential Equations*. Springer, 2011.
13. A. Hüppe and M. Kaltenbacher. Advanced spectral finite element method for computational acoustics in the mid-frequency range. In *Proceedings of the ISMA 2010*, 2010.
14. F. Brezzi and M. Fortin. *Mixed and Hybrid Finite Element Methods*. Springer, New York, 1991.
15. P. A. Raviart and J. M. Thomas. A mixed finite element method for 2nd order elliptic problems. *Mathematical Aspects of the Finite Element Method, Lecture Notes in Mathematics*, 606, 1977.
16. Y. Maday and C. Bernardi. *Spectral Methods, Handbook of Numerical Analysis, VOL. V*. Elsevier Science B.V., 1997.
17. Hüppe. Limits of finite element methods in the mid-frequency range. In *Proceedings of the DAGA'09*, pages 202–205, 2009. CD-ROM-Proceedings, Amsterdam.
18. Christopher K.W. Tam. Benchmark problems and solutions. In *ICASE/LaRC Workshop on Benchmark Problems in Computational Aeroacoustics*, 1995.
19. E-A. Müller and F. Obermeier. The spinning vortices as a source of sound. In *Fluids dynamics of Rotor and Fan supported Aircraft at Subsonic Speeds*, 1967.
20. T.F. Brooks, D. Pope, and Marcolini. Airfoil self-noise and prediction. *NASA Reference Publication 1218*, 1989.
21. Michele De Gennaro, Andreas Hueppe, Helmut Kuehnelt, and Manfred Kaltenbacher. Numerical prediction of laminar instability noise for naca 0012 aerofoil. In *Proceedings of the 6th Symposium on Numerical Analysis of Fluid Flow and Heat Transfer*, 2011.
22. M. Kaltenbacher. Advanced simulation tool for the design of sensors and actuators. In *Proc. Eurosensors XXIV*. Elsevier, 2010. CD-ROM-Proceedings, Linz.